Angewandte Chemie
Eine Zeitschrift der Gesellschaft Deutscher Chemiker

Supporting Information

Single-Bonded Cubic AsN from High-Pressure and High-Temperature Chemical Reactivity of Arsenic and Nitrogen

Matteo Ceppatelli, Demetrio Scelta, Manuel Serrano-Ruiz, Kamil Dziubek, Marta Morana, Volodymyr Svitlyk, Gaston Garbarino, Tomasz Poręba, Mohamed Mezouar, Maurizio Peruzzini, and Roberto Bini*

anie_202114191_sm_miscellaneous_information.pdf

Supporting Information

Contents

SI-1 Experimental section

Purification and recrystallization of arsenic. The arsenic lump was purchased from Alfa Aesar (99,999%). Pure crystalline rhombohedral As was recrystallized from grey-As according to a modification of the technique by Jeavons et al.[1] The polycrystalline sample (10-15 mg) was loaded in a quartz tube (length 10 cm, external diameter 13 mm, internal diameter 10 mm) under N_2 gas. The tube was sealed under vacuum, heated to 730 ℃ (2 ℃/min) and maintained at this temperature for 8 h, before slowly cooling it (0.06 ℃/min) to finally obtain high purity crystals (Figure SI-1). The sample was then loaded in a glovebox under Ar atmosphere. The purity of the recrystallized As was checked by single crystal and powder X-ray diffraction. Despite the declared purity of the purchased As being 99.999%, we found traces of As_2O_3 and further purified and recrystallized As. The results of the experiments were perfectly reproducible using either purchased or purified and recrystallized As, with no appreciated difference in terms of synthesis and characterization of the reaction product.

Sample preparation and the experimental conditions. Pressure was generated by means of membrane Diamond Anvil Cells (DAC) equipped with Ia type standard cut 16-sided beveled anvils having 300 μm culets. Re gaskets 200 μm thick were indented to 50 μm thickness and laser-drilled to obtain a 150 μm sample chamber. A small crystal of As was placed in the sample chamber and the remaining volume was filled with high purity (6.0) fluid N_2 using standard gas-loading technique. The equation of state (EOS) of a Au chip[2] and the ruby photoluminescence[3] were used to measure the pressure, whereas the temperature was measured by the fit of the black body thermal radiation emission of the sample during laser heating. High temperature (1050-1400 K) was generated by means of Nd:YAG laser source (λ=1064 nm, 15-20 W) focused on the As crystal (≈20-30 μm beam spot diameter), which acted both as reactant and laser absorber, thus avoiding any other source of contamination. No evidence of formation of Au or Re[4] nitrides was observed. A slight pressure increase of

1-3 GPa was observed after LH.

X-ray diffraction data acquisition and analysis. X-ray diffraction (XRD) experiments were carried out at the ESRF-ID27 (λ=0.3738 Å, MAR CCD165, sample to detector distance 379.1 mm) and ESRF-ID15B (λ=0.4104 Å, EIGER2 X CdTe 9M detector, sample to detector distance 179.5 mm) beamlines using a monochromatic synchrotron radiation focused to ∼5 μm to select different areas of the heterogeneous sample. The setup was calibrated against CeO_2 (ID27) and SiO_2 (ID15B) powder standards, using Dioptas[5] software for integrating the 2D area images to 1D patterns. Single crystal data sets were collected between 22.4 and 38.6 GPa. Diffraction intensities were acquired in an ω-oscillation scan mode ($\pm$30° range, 1.0° frame width, 2 s exposure per frame at ID27 and $\pm$32° range, 0.5° frame width, 0.4 s exposure per frame at ID15B). The instrument models were calibrated using enstatite single-crystal and the diffraction images were processed using a CrysAlisPro suite.[6] Additional panoramic oscillation images were acquired ($\phi = \pm 15°$, 20-30 s acquisition time, 9.8-50.5 GPa at ID27 and $\phi = \pm 32°$, 0.4 s acquisition time, 22.4-38.6 GPa at ID15B). Corrections for Lorentz and polarization effects, as well as multiscan absorption correction were applied to the intensity data. No evidence for twinning, satellite reflections or diffuse scattering was found at the visual inspection of the area detector images. The structure was solved by direct methods using SHELXT[7] and refined by full-matrix least-squares calculations using SHELXL program suite.[8]

SI-2 Results

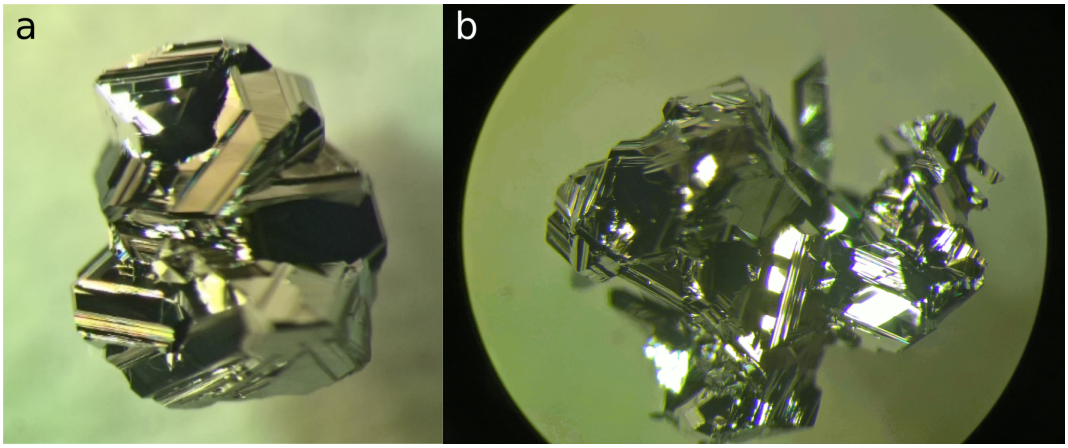

Figure SI-1: Microscope images of an As sample after purification and re-crystallization according to a modified version of the procedure described by Jeavons at al.[1]

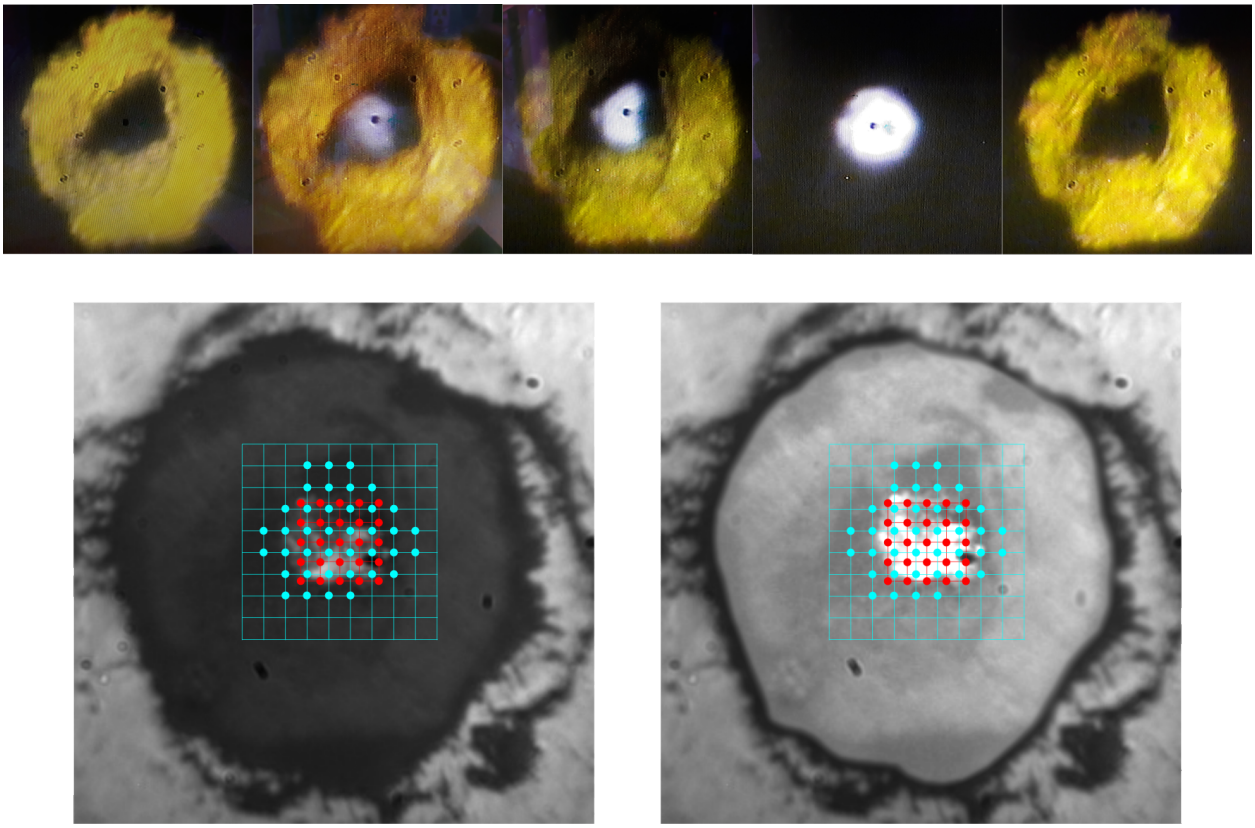

Figure SI-2: *Upper panels.* Images acquired before, during and after laser heating of As in N_2 at 14.7 GPa. The dark area at the center of the gasket hole is the As crystal, whereas the surrounding transparent area contains N_2. *Lower panels.* The same image of the sample (with higher exposure of the central part on the right) acquired after laser heating at 25 GPa. Two different XRD grid maps (cyan and red), superimposed to the images, represent the spots of the sample where XRD patterns were acquired, covering the entire As chip and extending into the surrounding N_2 area. The solid circles (red and cyan) indicate sample spots where the reaction product AsN was observed.

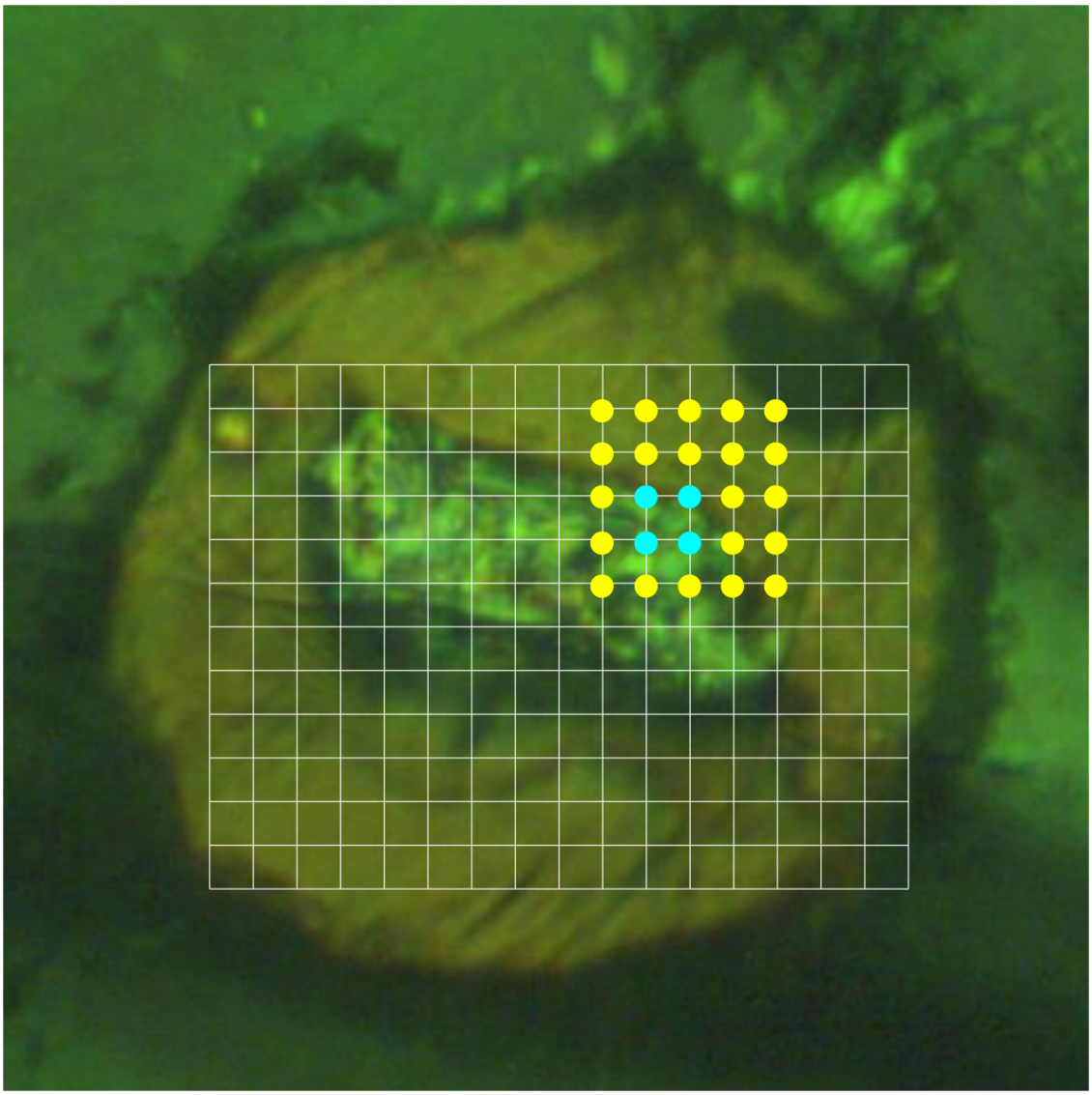

Figure SI-3: Microscope images of a sample of As (As-II, sc) in ϵ-N_2 acquired at 38.6 GPa and 293 K after laser heating at 36.0 GPa. The white grid (5 μm spacing) indicates a XRD panoramic mapping of the sample, whereas the smaller yellow grid (5 μm spacing) and points indicate the spots where single crystal acquisitions were performed, with the cyan points highlighting the detection of the single crystal AsN product. A ruby and a Au chip used for the pressure measurement are also visible near the gasket, respectively on the top left and top right sides of the gasket hole.

Chemical formula	AsN	AsN	AsN	AsN	AsN	AsN
P_{Au} (GPa)	-	37.4	35.3	32.5	29.6	26.6
P_{ruby} (GPa)	38.6	38.2	35.9	33.3	30.3	27.7
$P_{Au-ruby}$ (GPa)	38.6	37.8	35.6	32.9	30.0	27.2
Temperature (K)	293	293	293	293	293	293
Crystalline system	Cubic	Cubic	Cubic	Cubic	Cubic	Cubic
Space group	$P2_13$ (n. 198)	$P2_13$ (n. 198)	$P2_13$ (n. 198)	$P2_13$ (n. 198)	$P2_13$ (n. 198)	-
a (Å)	8.6884(2)	8.6820(3)	8.7024(4)	8.7297(9)	8.7677(12)	8.8128(12)
α (°)	90	90	90	90	90	90
V (Å^3)	655.88(5)	654.42(7)	659.06(10)	665.3(2)	674.0(3)	684.4(3)
Z	32	32	32	32	32	-
density (g cm^{-3})	7.205	7.221	7.170	7.103	7.011	6.904
Wavelength (Å)	0.41047	0.41047	0.41047	0.41047	0.41047	0.41047
No. of m, i, o [I $> 2\sigma$(I)] reflections	1599, 796, 542	1581, 791, 633	1605, 804, 650	1649, 820, 521	1643, 826, 507	-
R_{int}	0.030	0.030	0.023	0.030	0.053	-
Final R1, wR2 indices [I $> 2\sigma$(I)]	0.047, 0.107	0.047, 0.105	0.040, 0.082	0.041, 0.080	0.054, 0.120	-
Final R1, wR2 indices [all data]	0.069, 0.119	0.058, 0.110	0.053, 0.086	0.068, 0.086	0.097, 0.138	-
S	0.951	0.995	0.982	0.836	0.924	-
No. of parameters	49	49	49	49	49	-

Table SI-1: Selected refinement parameters for AsN at different pressure values. m, i, o respectively indicate measured, independent and observed reflections. P_{Au} indicates the pressure value measured by the Au EOS,[2] P_{ruby} indicates the pressure value measured by the ruby photoluminescence scale[3] and $P_{Au-ruby}$ indicates the average (when possible) of the Au and ruby pressure values. For the data point corresponding to 27.2 GPa only the unit cell parameters, with no refinement of the atomic positions, could be obtained.

SI-4 Distances and angles

The three N-As-N angles at two types of As atoms (As01 and As02 in Table SI-2) are not identical, as attested by the two angles with $\lesssim$90° value and by the one with >95° value. This occurrence indicates a slightly asymmetric coordination environment for these two As atoms, leading to a distortion of the corresponding AsN_3 trigonal pyramids. However, within the trivalent connection scheme, the average values of the three N-As-N angles at each of the four As atoms are perfectly consistent with the values expected for trivalent trigonal-pyramidal coordinated As hosting an expressed electron lone pair. This observation is further supported by the results by Tolborg et al. reporting connected YX_3 (Y=Sb) units to have smaller X-Y-X angles than the isolated ones[9] and higher electron lone pair expression. In agreement with this observation two of the average N-As-N angles in AsN have comparable or slightly smaller values (91.3-92.0°and 92.0-92.7°) in the explored pressure range with respect to the H-As-H angle (91.8°at ambient conditions) of AsH_3,[10] despite the larger steric hindrance of N compared to H.

Table SI-2: Lattice parameter, unit cell volume, interatomic distances and angles of AsN obtained from single crystal refinement of datasets acquired at different pressure points. P_{Au} indicates the pressure value measured by the Au EOS,[2] P_{ruby} indicated the pressure value measured by the ruby photoluminescence scale[3] and $P_{Au-ruby}$ indicates the average (when possible) of the Au and ruby pressure values. The symmetry codes for the atomic positions are listed in Table SI-4.

P_{Au} (GPa)	-	37.4	35.3	32.5	29.6
P_{ruby} (GPa)	38.6	38.2	35.9	33.3	30.3
$P_{Au-ruby}$ (GPa)	38.6	37.8	35.6	32.9	30.0
a(Å)	8.6884(2)	8.6820(3)	8.7024(4)	8.7297(9)	8.7677(12)
V(Å)	655.88(5)	654.42(7)	659.06(10)	665.3(2)	674.0(3)
interatomic distances (Å)					
As01-N01^{i}	1.864(12)	1.895(9)	1.888(8)	1.870(13)	1.875(14)
As01-N02^{ii}	1.860(12)	1.856(9)	1.859(8)	1.859(11)	1.858(12)
As01-N03	1.854(7)	1.855(5)	1.849(4)	1.857(6)	1.853(7)
As02-N01^{iii}	1.854(11)	1.842(9)	1.849(7)	1.845(11)	1.856(12)
As02-N02^{iv}	1.913(12)	1.916(9)	1.916(8)	1.908(12)	1.923(13)
As02-N04^{v}	1.872(5)	1.870(4)	1.876(3)	1.871(5)	1.875(5)
As03-N01, As03-N01^{i}, As03-N01^{vi}	1.865(12)	1.857(9)	1.861(8)	1.870(13)	1.866(14)
As04-N02^{vii}, As04-N02^{viii}, As04-N02^{ix}	1.872(12)	1.867(9)	1.870(8)	1.879(13)	1.879(14)
As02$\cdots$As02^{x}, As02$\cdots$As02^{xi}	2.808(3)	2.805(2)	2.8134(18)	2.829(3)	2.848(3)
As04$\cdots$As01^{vii}, As04$\cdots$As01^{viii}, As04$\cdots$As01^{ix}	2.807(3)	2.801(2)	2.8115(19)	2.831(3)	2.849(3)
valence angles (°)					
N01^{i}-As01-N02^{ii}	89.4(6)	88.9(4)	89.1(4)	89.6(7)	90.0(7)
N01^{i}-As01-N03	92.5(6)	92.4(4)	92.1(4)	92.9(5)	92.3(7)
N02^{ii}-As01-N03	98.7(5)	98.5(3)	99.0(3)	99.4(4)	99.5(5)
N01^{iii}-As02-N02^{iv}	89.7(6)	90.1(4)	90.1(4)	89.8(7)	90.1(7)
N01^{iii}-As02-N04^{v}	92.9(5)	93.8(4)	93.3(4)	93.4(6)	93.7(6)
N02^{iv}-As02-N04^{v}	93.3(4)	93.2(4)	93.2(3)	93.7(5)	94.2(5)
N01-As03-N01^{i}, N01-As03-N01^{vi}, N01^{i}-As03-N01^{vi}	93.0(5)	94.1(4)	93.8(3)	93.7(5)	93.7(5)
N02^{vii}-As04-N02^{viii}, N02^{vii}-As04-N02^{ix}, N02^{viii}-As04-N02^{ix}	91.3(5)	91.4(4)	91.3(3)	91.5(5)	92.0(5)
As01^{vi}-N01-As02^{ii}	109.2(6)	108.4(5)	108.7(4)	109.7(6)	109.5(6)
As01^{vi}-N01-As03	110.0(6)	108.9(4)	109.3(4)	110.0(6)	110.5(6)
As02^{ii}-N01-As03	110.1(6)	110.9(5)	110.7(4)	110.9(6)	110.9(7)
As01^{iii}-N02-As02^{xii}	103.4(6)	103.3(4)	103.4(4)	103.8(6)	103.3(6)
As01^{iii}-N02-As04^{xiii}	111.6(6)	112.0(5)	112.0(4)	111.8(6)	112.3(7)
As02^{xii}-N02-As04^{xiii}	107.9(6)	108.1(4)	108.1(4)	108.2(6)	107.9(6)
As01-N03-As01^{i}, As01-N03-As01^{vi}, As01^{i}-N03-As01^{vi}	107.3(6)	107.3(4)	108.0(3)	107.6(5)	108.4(6)
As02^{xiv}-N04-As02^{xv}, As02^{xv}-N04-As02^{xvi}, As02^{xiv}-N04-As02^{xvi}	112.7(4)	112.8(3)	112.6(3)	113.3(4)	113.6(4)

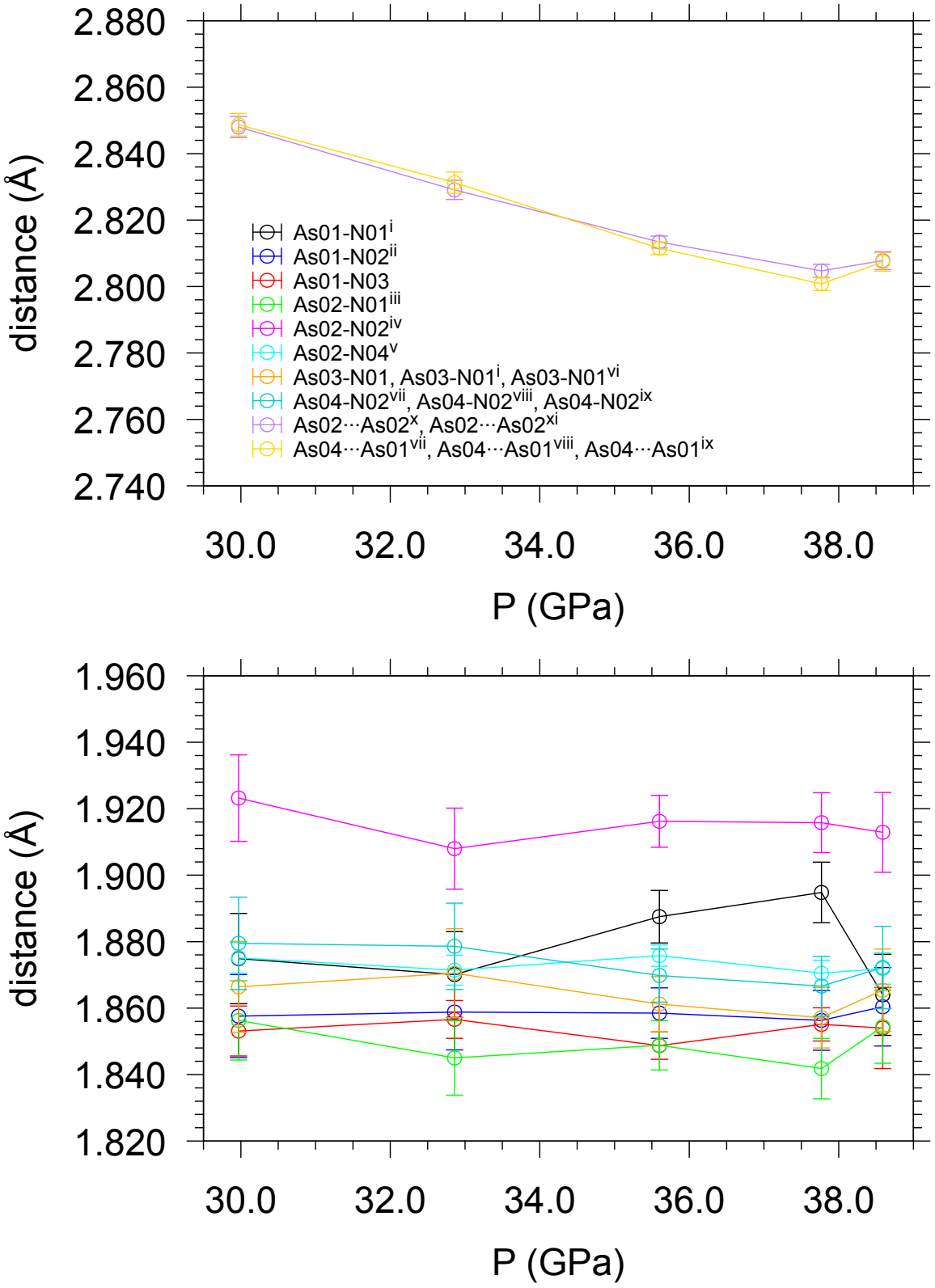

Figure SI-4: Pressure evolution of interatomic distances in the $P2_13$ cubic structure of AsN at room T in the 30-40 GPa pressure range. The caption in the upper panel accounts also for the data plotted in the lower one. The symmetry codes for the atomic positions are listed in Table SI-4.

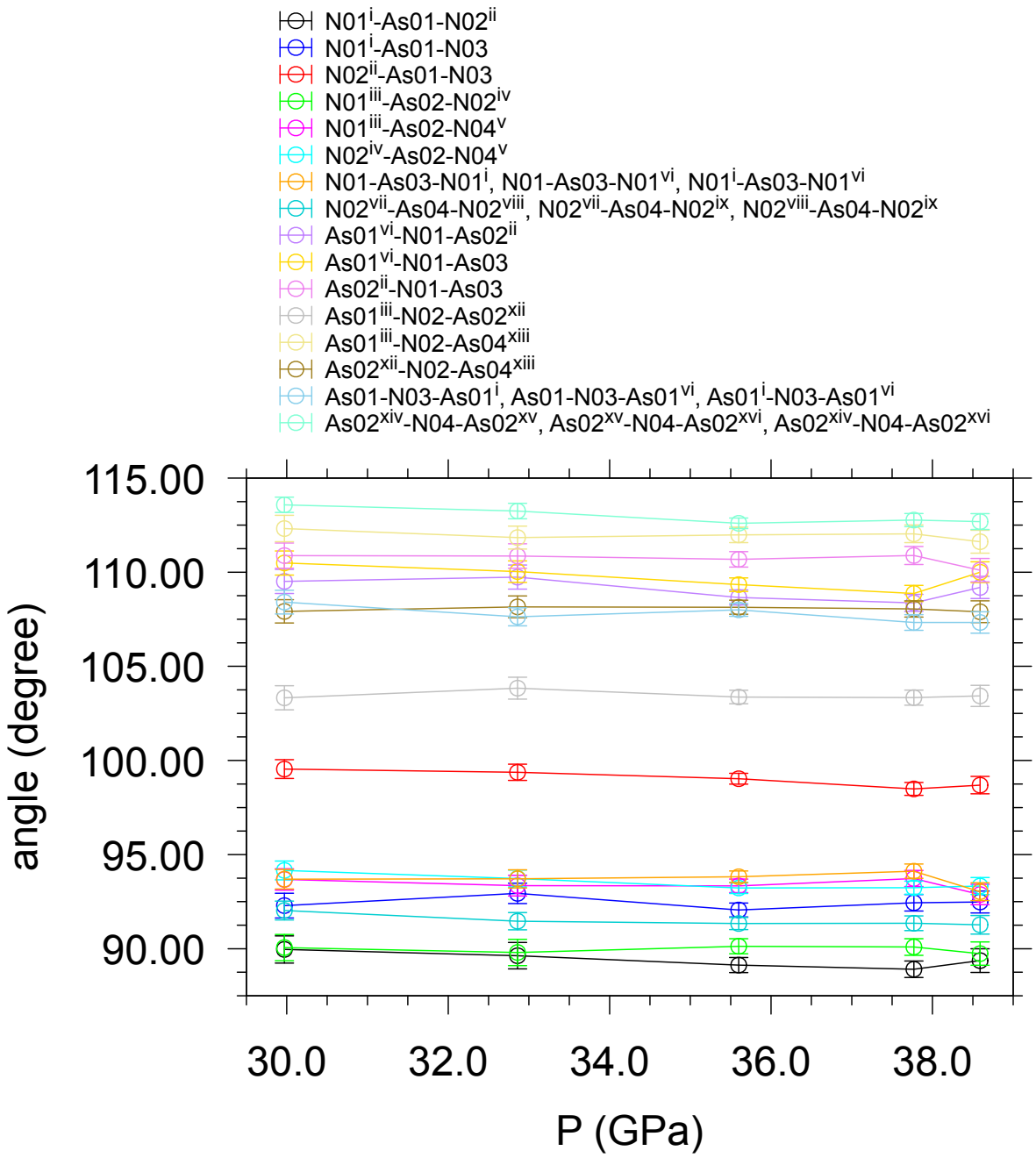

Figure SI-5: Pressure evolution of angles in the $P2_13$ cubic structure of AsN at room T in the 30-40 GPa pressure range. The symmetry codes for the atomic positions are listed in Table SI-4.

SI-5 As_4 tetrahedra

One type of the four As_4 tetrahedra is formed by one As04 at the apex and three As01 atoms at the base (As04$\cdots$As01=2.8116 Å, As01$\cdots$As01=2.9764 Å at 35.6 GPa and 293 K, Figure 5A). All the electron lone pairs of the four As atoms apparently point towards the center of the tetrahedron, while the electron lone pairs belonging to surrounding N atoms (N01) point towards the center of each tetrahedron face. In particular the electron lone pair of one N04 atom points towards the center of the tetrahedron base (As01-As01-As01) and those of three N01 atoms towards the center of the remaining three faces (As04-As01-As01). This electron lone pairs arrangement, made by two interpenetrating electron lone pairs tetrahedra respectively belonging to four As and four N atoms, actually sets up an optimal isotropic compression environment. As a matter of fact, all the distances between the four As atoms slightly decrease with pressure, whereas the angles of tetrahedron remain substantially unaffected (Figure SI-6).

A second type of As_4 tetrahedron is formed by one As03 atom at the apex and three As02 atoms at the base (As03$\cdots$As02=2.9351 Å, As02$\cdots$As02=3.1211 Å, at 35.6 GPa and 293 K, Figure 5B). In this case the three As atoms (As02) at the base of the tetrahedron are bonded to the same N atom (N04), actually forming a NAs_3 pyramid. Only the electron lone pair of one As atom (As03) at the apex points to the center of the tetrahedron, whereas the electron lone pairs of the other three As02 atoms are oriented outside the tetrahedron along its As03-As02-As02 faces, slightly tilted with respect to the direction of the C_3 axis containing the As03 and its lone pair. Among the electron lone pairs of the surrounding N atoms, three of them (N02) point towards the center of the tetrahedron faces (As03-As02-As02), whereas the fourth one (N04) points outside the tetrahedron perpendicularly to its base, along the direction of the C_3 axis which contains also the As04 atom. In this case the distances between the As02 atoms at the base of the tetrahedron and the As03 atom at its apex decrease more with pressure than the distances between the As02 atoms, which are connected by strong rigid covalent bonds to the common N04 atom (Figure SI-7). Consistently, whereas the three

As02-As02-As02 angles at the tetrahedron base remain almost constant with pressure, the two As03-As02-As02 angles, formed by each of the three side faces with the tetrahedron base, slightly decrease with pressure and the three As02-As03-As02 angles at the apex of each side face markedly increase on compression, indicating a flattening of the tetrahedron.

A third type of As_4 tetrahedron is formed by one As04 atom at the apex and three As02 atoms at the base (As04$\cdots$As02=3.0657 Å, As02$\cdots$As02=2.8134 Å, at 35.6 GPa and 293 K, Figure 5C). The As04 atom is connected to the three As02 atoms by corresponding bridging N atoms (N02), but no chemical bond connects the three As02 atoms. In this atomic arrangement none of the electron lone pairs belonging to the As atoms point towards the center of the tetrahedron, nor those belonging to the surrounding N atoms (N02) point to its faces. In particular, the electron lone pairs of the three As02 atoms and those of the three N02 atoms are arranged almost perpendicularly to the C_3 axis containing the As04 atom, with opposite rotation direction around it, apparently adopting this arrangement to minimize their directional repulsive interaction. In this third type of As_4 tetrahedron the distances between the As02 atoms at the base of the tetrahedron decrease more with pressure than the their distances to the As04 atom at the apex of the tetrahedron, as expected from the absence of chemical bonds between the first ones and from the presence of covalently bonded N02 atoms bridging the last ones. While the three As02-As02-As02 angles at the tetrahedron base remain constant with pressure due to symmetry constraints, the two As04-As02-As02 angles at each of the three side faces of the tetrahedron slightly increase with pressure, whereas the three As02-As04-As02 angles at the apex of each side face slightly decrease on compression, indicating in this case a sharpening of the tetrahedron, consistently with the absence of electron density at its center (Figure SI-8).

A fourth type of As_4 tetrahedron is formed by one As03 atom at the apex and three As01 atoms at the base (As03$\cdots$As01=3.058 Å, As01$\cdots$As01=2.991 Å, at 35.6 GPa and 293 K, Figure 5C). The As03 atom is connected to the three As01 atoms by corresponding bridging N atoms (N01). The three As atoms (As01) at the base of the tetrahedron are bonded to

the same N atom (N03), actually forming a NAs_3 pyramid. It is worth to note that the electron lone pair of the N03 atom points to the center of the base (As02-As02-As02) of the third type of As_4 tetrahedron (As04-As02-As02-As02), for which, as already mentioned, the electron lone pairs of the other three bridging N01 atoms, are oriented outside its side (As04-As01-As01) faces. In this fourth type of As_4 tetrahedron the two types of As$\cdots$As distances decrease comparably on compression, while the As-As-As angles remain essentially constant (Figure SI-9). This behavior is consistent with the rigid covalent framework of a closed As_4N_4 cage-like structure, where all As atoms are bridged by the N ones, with all the electron lone pairs pointing outside it.

Table SI-3: Interatomic distances and angles of the three different As_4 tetrahedra identified in the AsN structure from single crystal refinement of datasets acquired at different pressure points. P_{Au} indicates the pressure value measured by the Au EOS,[2] P_{ruby} indicated the pressure value measured by the ruby photoluminescence scale[3] and $P_{Au-ruby}$ indicates the average (when possible) of the Au and ruby pressure values. The symmetry codes for the atomic positions are listed in Table SI-4.

Pattern	AsN2x3_0313	AsN2x3_b_0040	AsN2x3_b_0053	AsN2x3_b_0055	AsN2x3_b_0057
P_{Au} (GPa)	-	37.4	35.3	32.5	29.6
P_{ruby} (GPa)	38.6	38.2	35.9	33.3	30.3
$P_{Au-ruby}$ (GPa)	38.6	37.8	35.6	32.9	30.0
a(Å)	8.6884(2)	8.6820(3)	8.7024(4)	8.7297(9)	8.7677(12)
V(Å)	655.88(5)	654.42(7)	659.06(10)	665.3(2)	674.0(3)
interatomic As$\cdots$As distances (Å) and As-As-As angles (degree) of the As04-As01-As01-As01 tetrahedron					
As01$\cdots$As04^{xiii}	2.807(3)	2.801(2)	2.8116(19)	2.831(3)	2.849(3)
As01$\cdots$As01^{xvii}	2.967(2)	2.9617(17)	2.9763(14)	2.991(2)	3.014(3)
As01$\cdots$As01^{xviii}	2.967(2)	2.9617(17)	2.9763(14)	2.991(2)	3.014(3)
As04$^{xiii}\cdots$As01^{xvii}	2.807(3)	2.801(2)	2.8116(19)	2.831(3)	2.849(3)
As04$^{xiii}\cdots$As01^{xviii}	2.807(3)	2.801(2)	2.8116(19)	2.831(3)	2.849(3)
As01$^{xvii}\cdots$As01^{xviii}	2.967(2)	2.9617(17)	2.9763(14)	2.991(2)	3.014(3)
As04^{xiii}-As01-As01^{xvii}	58.10(4)	58.08(3)	58.04(3)	58.11(4)	58.06(5)
As04^{xiii}-As01-As01^{xviii}	58.10(4)	58.08(3)	58.04(3)	58.11(4)	58.06(5)
As01^{xvii}-As01-As01^{xviii}	60	60	60	60	60
As01-As04^{xiii}-As01^{xvii}	63.80(8)	63.84(6)	63.92(5)	63.77(9)	63.89(9)
As01-As04^{xiii}-As01^{xviii}	63.80(8)	63.84(6)	63.92(5)	63.77(9)	63.89(9)
As01^{xvii}-As04^{xiii}-As01^{xviii}	63.80(8)	63.84(6)	63.92(5)	63.77(9)	63.89(9)
As01-As01^{xvii}-As04^{xiii}	58.10(4)	58.08(3)	58.04(3)	58.11(4)	58.06(5)
As01-As01^{xvii}-As01^{xviii}	60	60	60	60	60
As04^{xiii}-As01^{xvii}-As01^{xviii}	58.10(4)	58.08(3)	58.04(3)	58.11(4)	58.06(5)
As01-As01^{xviii}-As04^{xiii}	58.10(4)	58.08(3)	58.04(3)	58.11(4)	58.06(5)
As01-As01^{xviii}-As01^{xvii}	60	60	60	60	60
As04^{xiii}-As01^{xviii}-As01^{xvii}	58.10(4)	58.08(3)	58.04(3)	58.11(4)	58.06(5)
interatomic As$\cdots$As distances (Å) and As-As-As angles (degree) of the As03-As02-As02-As02 tetrahedron					
As03$\cdots$As02^{xix}	2.924(3)	2.9262(2)	2.9351(18)	2.947(3)	2.9738(3)
As03$\cdots$As02^{xx}	2.924(3)	2.9262(2)	2.9351(18)	2.947(3)	2.9738(3)
As03$\cdots$As02^{xxi}	2.924(3)	2.9262(2)	2.9351(18)	2.947(3)	2.9738(3)
As02$^{xix}\cdots$As02^{xx}	3.116(2)	3.1154(18)	3.1211(15)	3.126(3)	3.138(3)
As02$^{xix}\cdots$As02^{xxi}	3.116(2)	3.1154(18)	3.1211(15)	3.126(3)	3.138(3)
As02$^{xx}\cdots$As02^{xxi}	3.116(2)	3.1154(18)	3.1211(15)	3.126(3)	3.138(3)
As02^{xix}-As03-As02^{xx}	64.39(7)	64.33(5)	64.24(5)	64.04(8)	63.68(8)
As02^{xix}-As03-As02^{xxi}	64.39(7)	64.33(5)	64.24(5)	64.04(8)	63.68(8)
As02^{xx}-As03-As02^{xxi}	64.39(7)	64.33(5)	64.24(5)	64.04(8)	63.68(8)
As03-As02^{xix}-As02^{xx}	57.81(4)	57.84(3)	57.88(2)	57.98(4)	58.16(4)
As03-As02^{xix}-As02^{xxi}	57.81(4)	57.84(3)	57.88(2)	57.98(4)	58.16(4)
As02^{xx}-As02^{xix}-As02^{xxi}	60	60	60	60	60
As03-As02^{xx}-As02^{xix}	57.81(4)	57.84(3)	57.88(2)	57.98(4)	58.16(4)
As03-As02^{xx}-As02^{xxi}	57.81(4)	57.84(3)	57.88(2)	57.98(4)	58.16(4)
As02^{xix}-As02^{xx}-As02^{xxi}	60	60	60	60	60
As03-As02^{xxi}-As02^{xix}	57.81(4)	57.84(3)	57.88(2)	57.98(4)	58.16(4)
As03-As02^{xxi}-As02^{xx}	57.81(4)	57.84(3)	57.88(2)	57.98(4)	58.16(4)
As02^{xix}-As02^{xxi}-As02^{xx}	60	60	60	60	60
interatomic As$\cdots$As distances (Å) and As-As-As angles (degree) of the As04-As02-As02-As02 tetrahedron					
As02$\cdots$As02^{x}	2.808(3)	2.805(2)	2.8134(18)	2.829(3)	2.848(3)
As02$\cdots$As02^{xi}	2.808(3)	2.805(2)	2.8134(18)	2.829(3)	2.848(3)
As02$\cdots$As04^{vii}	3.060(4)	3.061(3)	3.066(2)	3.067(4)	3.075(4)
As02$^{x}\cdots$As02^{xi}	2.808(3)	2.805(2)	2.813(2)	2.829(3)	2.848(3)
As02$^{x}\cdots$As04^{vii}	3.060(4)	3.061(3)	3.066(2)	3.067(4)	3.075(4)
As02$^{xi}\cdots$As04^{vii}	3.060(4)	3.061(3)	3.066(2)	3.067(4)	3.075(4)
As02^{x}-As02-As02^{xi}	60	60	60	60	60
As02^{x}-As02-As04^{vii}	62.69(3)	62.73(2)	62.69(2)	62.53(3)	62.41(4)
As02^{xi}-As02-As04^{vii}	62.69(3)	62.73(2)	62.69(2)	62.53(3)	62.41(4)
As02-As02^{x}-As02^{xi}	60	60	60	60	60
As02-As02^{x}-As04^{vii}	62.69(3)	62.73(2)	62.69(2)	62.53(3)	62.41(4)
As02^{xi}-As02^{x}-As04^{vii}	62.69(3)	62.73(2)	62.69(2)	62.53(3)	62.41(4)
As02-As02^{xi}-As02^{x}	60	60	60	60	60
As02-As02^{xi}-As04^{vii}	62.69(3)	62.73(2)	62.69(2)	62.53(3)	62.41(4)
As02^{x}-As02^{xi}-As04^{vii}	62.69(3)	62.73(2)	62.69(2)	62.53(3)	62.41(4)
As02-As04^{vii}-As02^{x}	54.61(6)	54.53(5)	54.63(4)	54.94(7)	55.17(7)
As02-As04^{vii}-As02^{xi}	54.61(6)	54.53(5)	54.63(4)	54.94(7)	55.17(7)
As02^{x}-As04^{vii}-As02^{xi}	54.61(6)	54.53(5)	54.63(4)	54.94(7)	55.17(7)
interatomic As$\cdots$As distances (Å) and As-As-As angles (degree) of the< As03-As01-As01-As01 tetrahedron					
As03$\cdots$As01	3.055(3)	3.052(2)	3.058(2)	3.065(4)	3.074(4)
As03$\cdots$As01^{i}	3.055(3)	3.052(2)	3.058(2)	3.065(4)	3.074(4)
As03$\cdots$As01^{vi}	3.055(3)	3.052(2)	3.058(2)	3.065(4)	3.074(4)
As01$\cdots$As01^{i}	2.987(3)	2.989(2)	2.991(2)	2.997(3)	3.006(3)
As01$\cdots$As01^{vi}	2.987(3)	2.989(2)	2.991(2)	2.997(3)	3.006(3)
As01$^{i}\cdots$As01^{vi}	2.987(3)	2.989(2)	2.991(2)	2.997(3)	3.006(3)
As01-As03-As01^{i}	58.53(6)	58.63(4)	58.55(4)	58.55(7)	58.55(7)
As01-As03-As01^{vi}	58.53(6)	58.63(4)	58.55(4)	58.55(7)	58.55(7)
As01^{i}-As03-As01^{vi}	58.53(6)	58.63(4)	58.55(4)	58.55(7)	58.55(7)
As03-As01-As01^{i}	60.73(3)	60.68(2)	60.72(2)	60.73(3)	60.73(4)
As03-As01-As01^{vi}	60.73(3)	60.68(2)	60.72(2)	60.73(3)	60.73(4)
As01^{i}-As01-As01^{vi}	60	60	60	60	60
As03-As01^{i}-As01	60.73(3)	60.68(2)	60.72(2)	60.73(3)	60.73(4)
As03-As01^{i}-As01^{vi}	60.73(3)	60.68(2)	60.72(2)	60.73(3)	60.73(4)
As01-As01^{i}-As01^{vi}	60	60	60	60	60
As03-As01^{vi}-As01	60.73(3)	60.68(2)	60.72(2)	60.73(3)	60.73(4)
As03-As01^{vi}-As01^{i}	60.73(3)	60.68(2)	60.72(2)	60.73(3)	60.73(4)
As01-As01^{vi}-As01^{i}	60	60	60	60	60

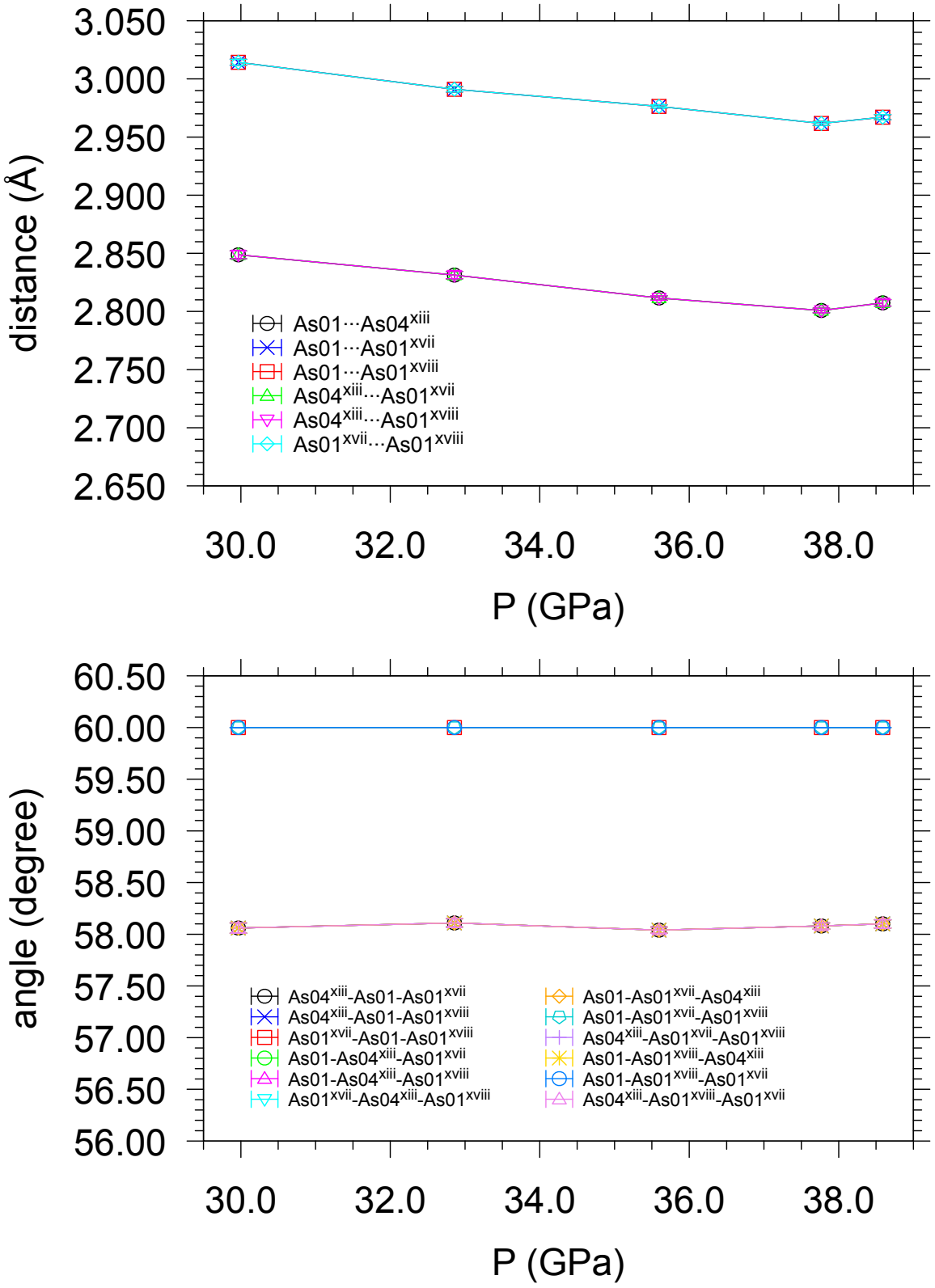

Figure SI-6: Pressure evolution of the As$\cdots$As distances and As-As-As angles of the As04-As01-As01-As01 tetrahedron (first type) in the $P2_13$ cubic structure of AsN at room T in the 30-40 GPa pressure range. The symmetry codes for the atomic positions are listed in Table SI-4.

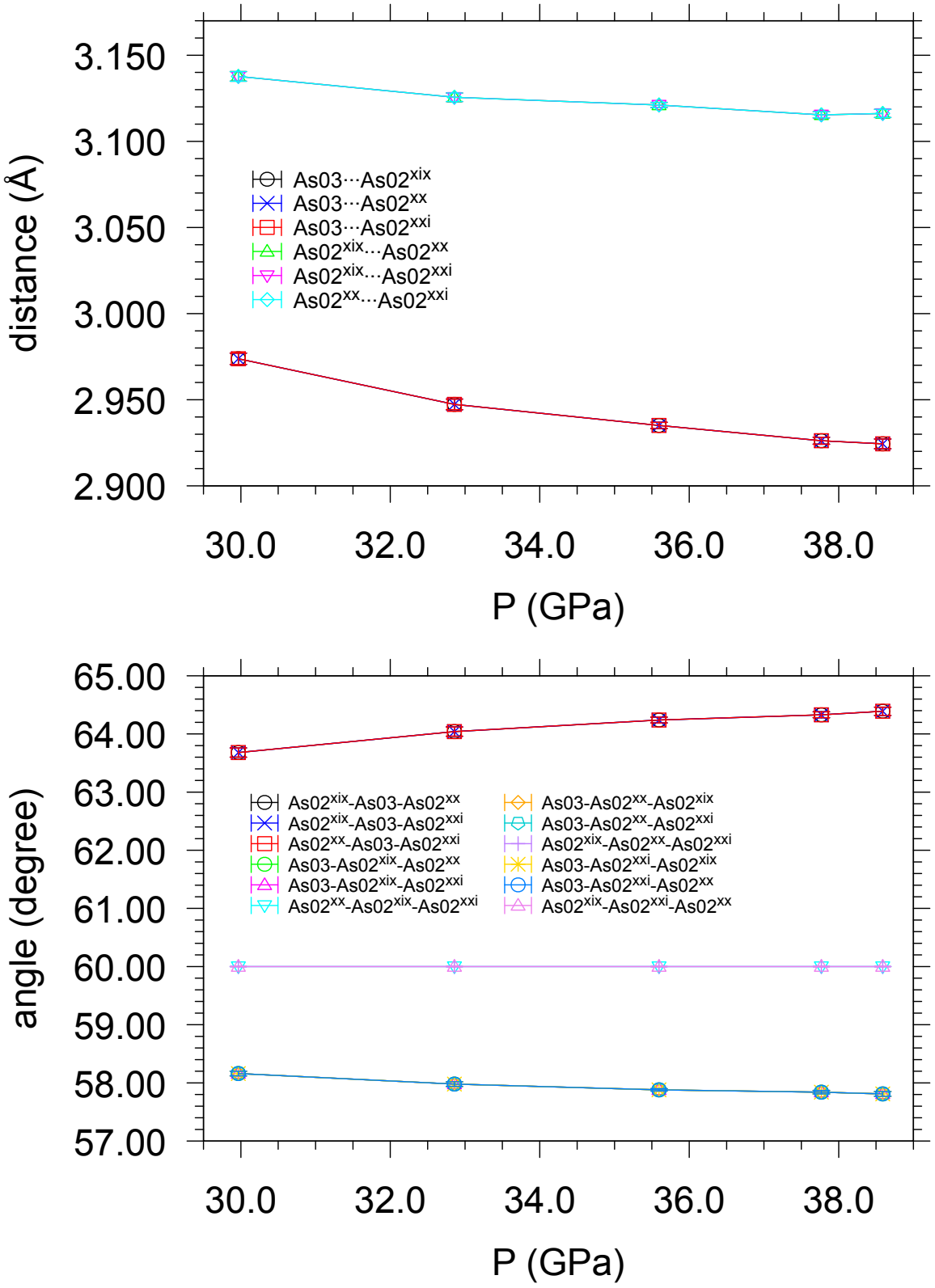

Figure SI-7: Pressure evolution of the As$\cdots$As distances and As-As-As angles of the As03-As02-As02-As02 tetrahedron (second type) in the $P2_13$ cubic structure of AsN at room T in the 30-40 GPa pressure range. The symmetry codes for the atomic positions are listed in Table SI-4.

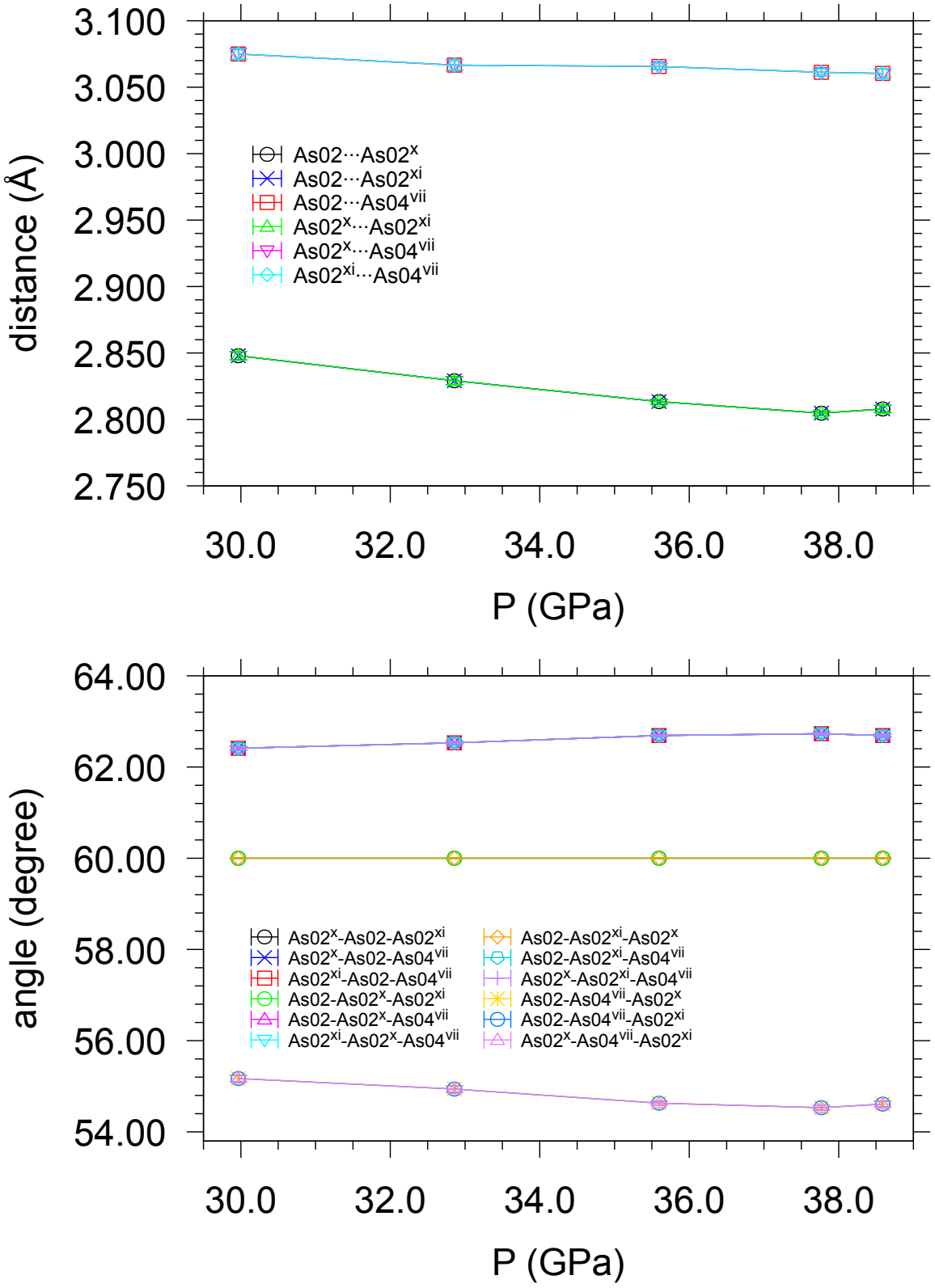

Figure SI-8: Pressure evolution of the As$\cdots$As distances and As-As-As angles of the As04-As02-As02-As02 tetrahedron (third type) in the $P2_13$ cubic structure of AsN at room T in the 30-40 GPa pressure range. The symmetry codes for the atomic positions are listed in Table SI-4.

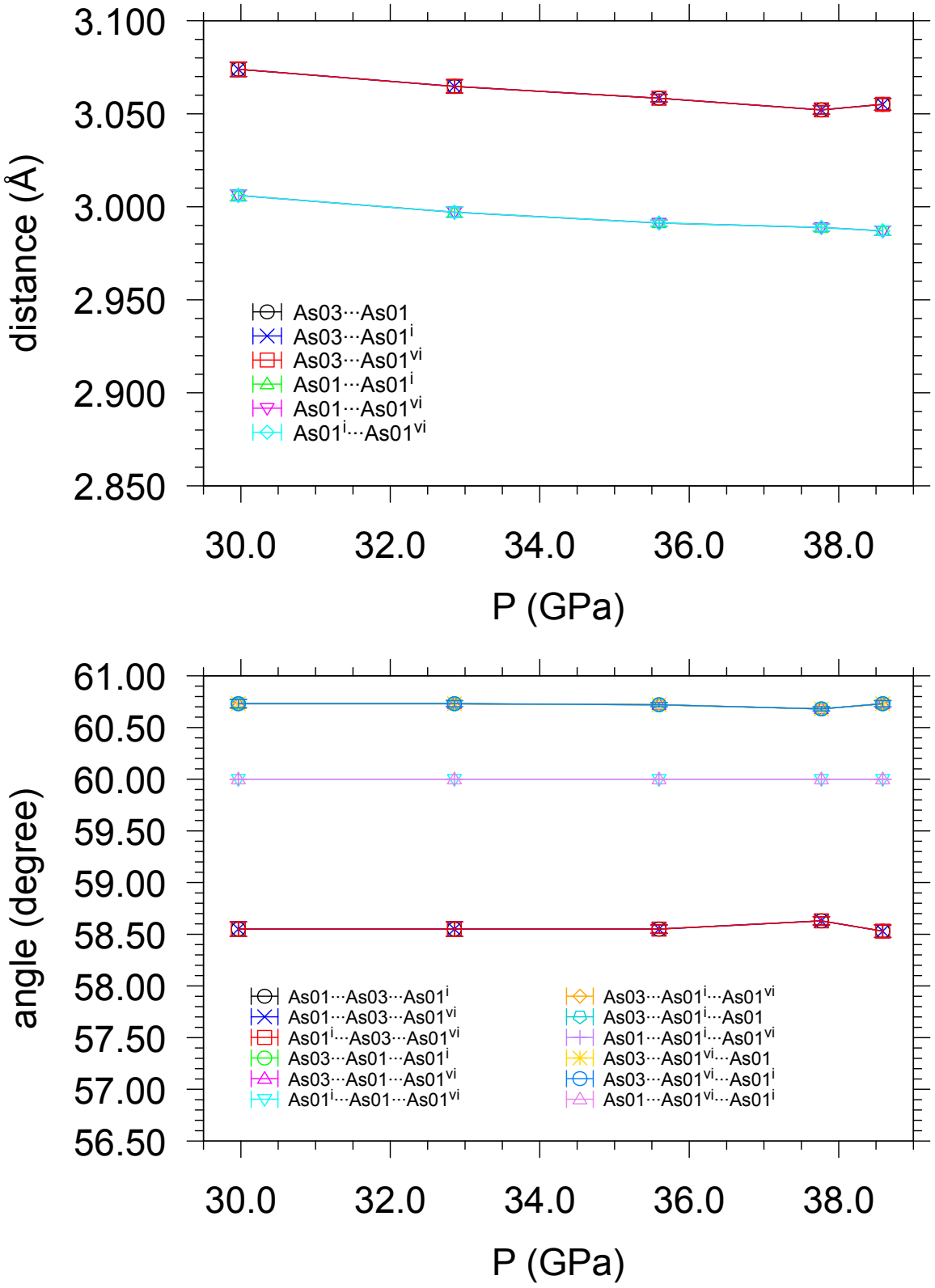

Figure SI-9: Pressure evolution of the As$\cdots$As distances and As-As-As angles of the As03-As01-As01-As01 tetrahedron (fourth type) in the $P2_13$ cubic structure of AsN at room T in the 30-40 GPa pressure range. The symmetry codes for the atomic positions are listed in Table SI-4.

Table SI-4: Symmetry codes for the atomic positions of the $P2_13$ (Z=32) unit cell of AsN.

i = z, x, y
ii = x-0.5, -y+0.5, -z
iii = x+0.5, -y+0.5, -z
iv = z+0.5, -x+1.5, -y
v = x, y, z-1
vi = y, z, x
vii = -x+1, y+0.5, -z+0.5
viii = -z+0.5, -x+1, y+0.5
ix = y+0.5, -z+0.5, -x+1
x = z+0.5, -x+1.5, -y+1
xi = -y+1.5, -z+1, x-0.5
xii = -y+1.5, -z, x-0.5
xiii = -x+1, y-0.5, -z+0.5
xiv = x, y, z+1
xv = z+1, x, y
xvi = y, z+1, x
xvii = z+0.5, -x+0.5, -y
xviii = -y+0.5, -z, x-0.5
xix = z, x-1, y-1
xx = y-1, z, x-1
xxi = x-1, y-1, z

SI-6 Additional volume data for AsN

Even if the data fitting procedure using a third order Birch-Murnaghan or Vinet equations of state converges, the limited number of data concentrated in the 30-40 GPa pressure interval, with no volume data at low pressure near the ambient pressure value, prevents a reliable fit of both dataset for the sample synthesized at 36.0 GPa and for the sample synthesized at 25.0 GPa.

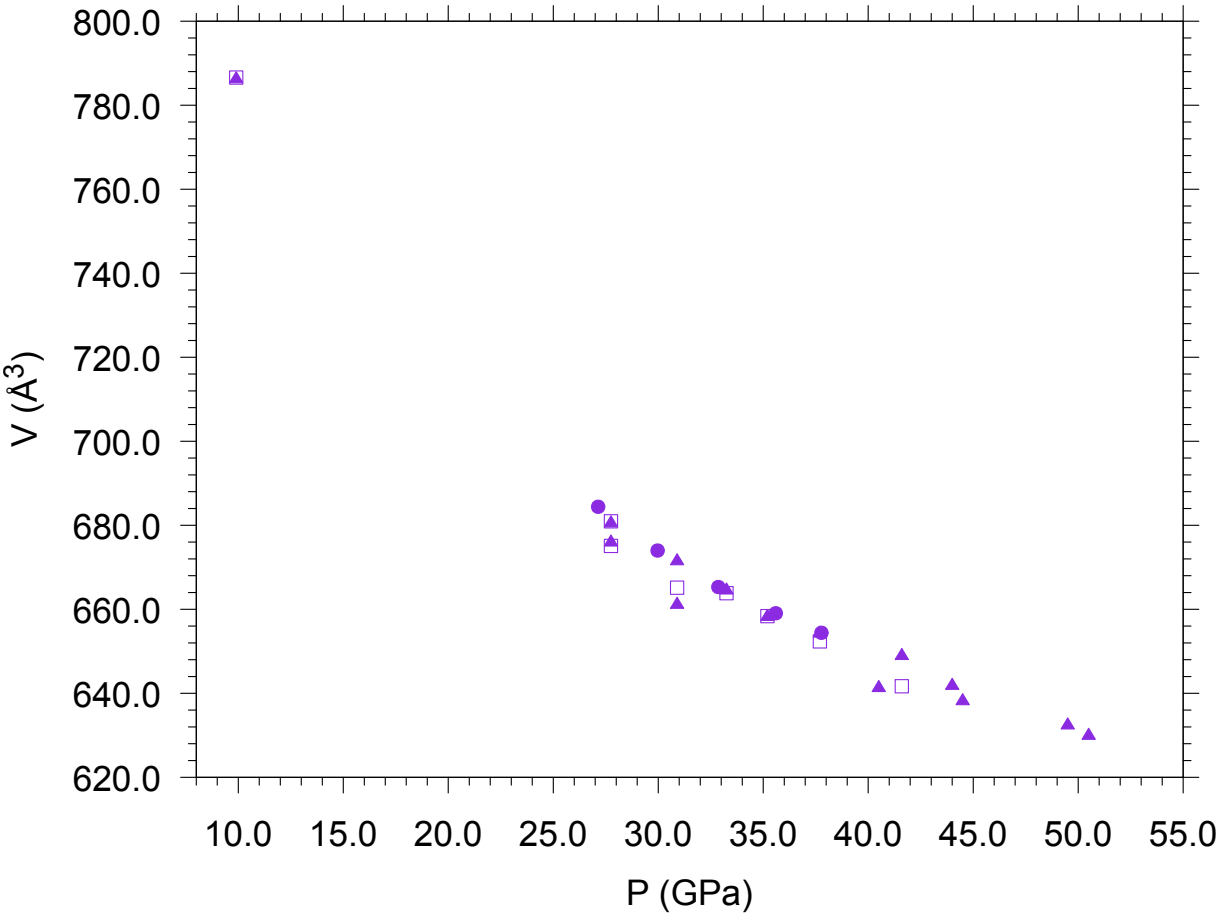

Figure SI-10: Pressure evolution of the unit cell volume of AsN at room T. The plotted data were acquired during the decompression of the sample synthesized at 25.0 GPa and derived respectively from the 111 and 211 reflections of the $P2_13$ unit cell of AsN observed in azimuthally integrated patterns.

SI-7 Structural chemistry of the $P2_13$ structure of AsN

The images of the AsN structure have been created using VESTA software.[11]

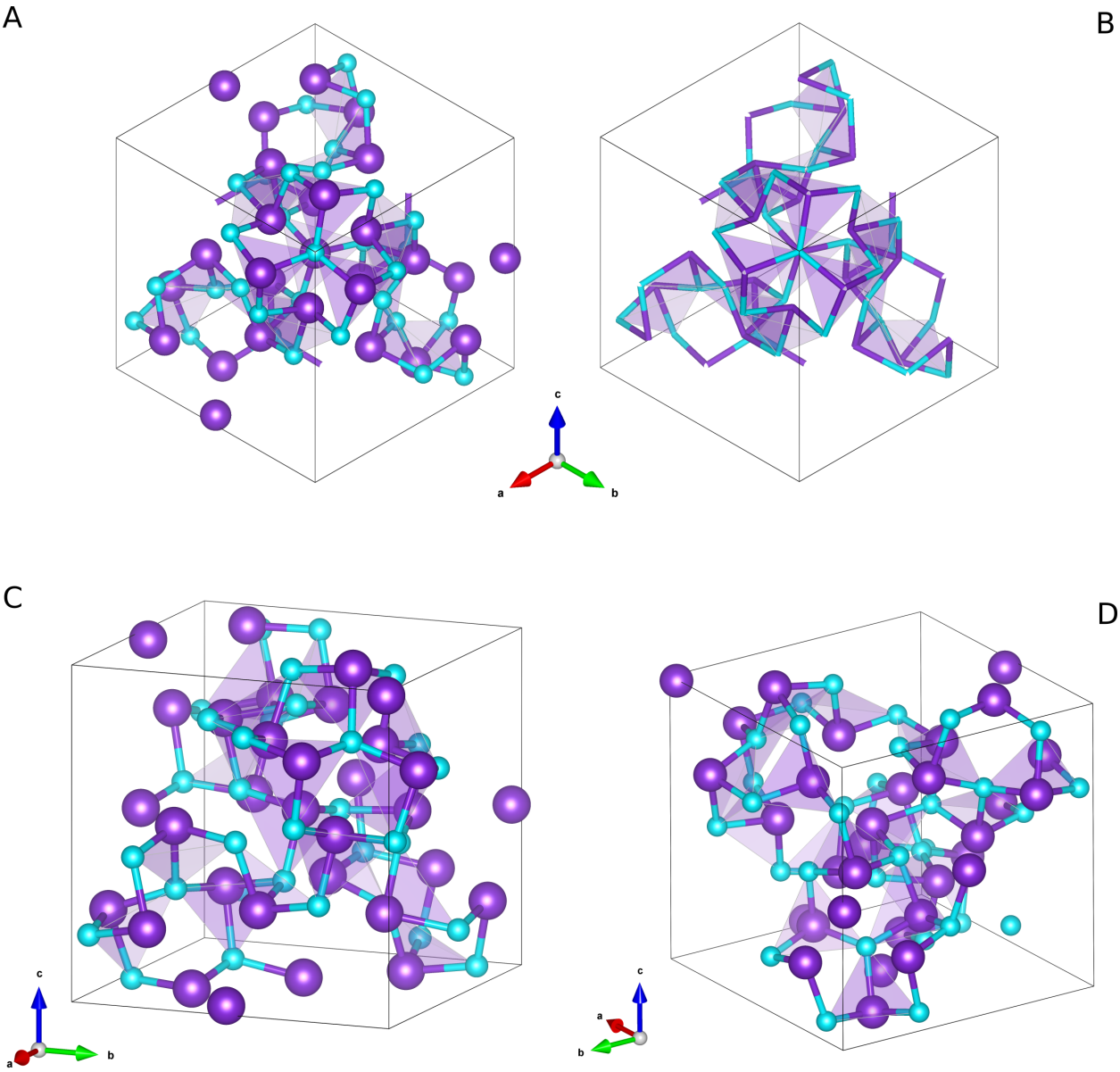

Figure SI-11: Different views of the $P2_13$ unit cell of AsN (As atoms in violet and N atoms in light blue) in the ball-stick (panels A, C, D) and stick (panel B) representation modes. The shaded polyhedra indicate the AsN_3 trigonal pyramids. Data refer to AsN at 35.6 GPa and 293 K.

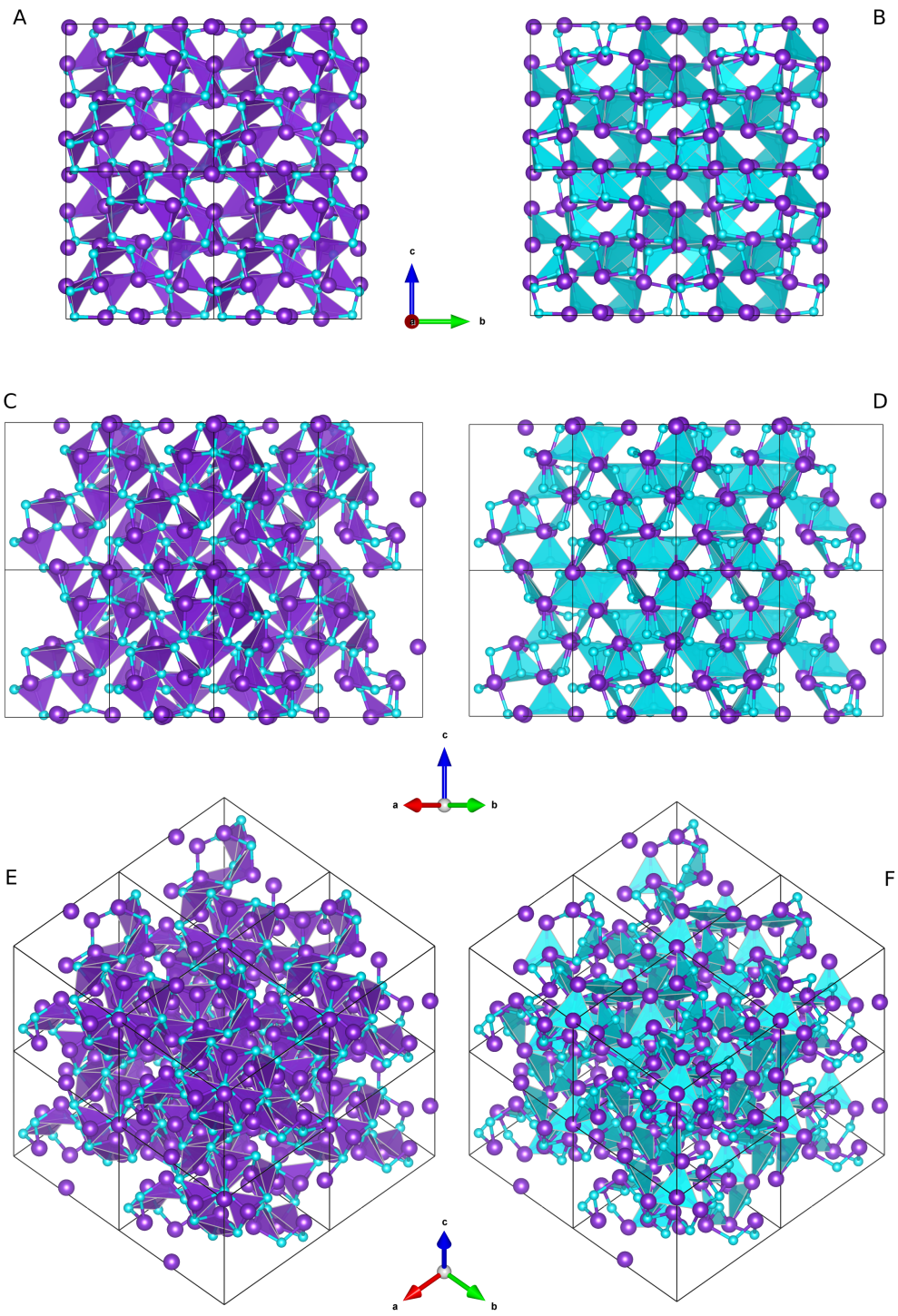

Figure SI-12: Views of the AsN structure (As atoms in violet and N atoms in light blue, 2x2x2 unit cells) along different crystallographic directions: [100] (panel A and B), [110] (panel C and D), one of the C_3 axis directed along [111] (panel E and F). The shaded polyhedra respectively indicate the AsN_3 (left, violet) and NAs_3 (right, blue) trigonal pyramids. The voids in the left and right images along the same view correspondingly highlight the presence of channels and cavities hosting lone pair electron density. Data refer to AsN at 35.6 GPa and 293 K.

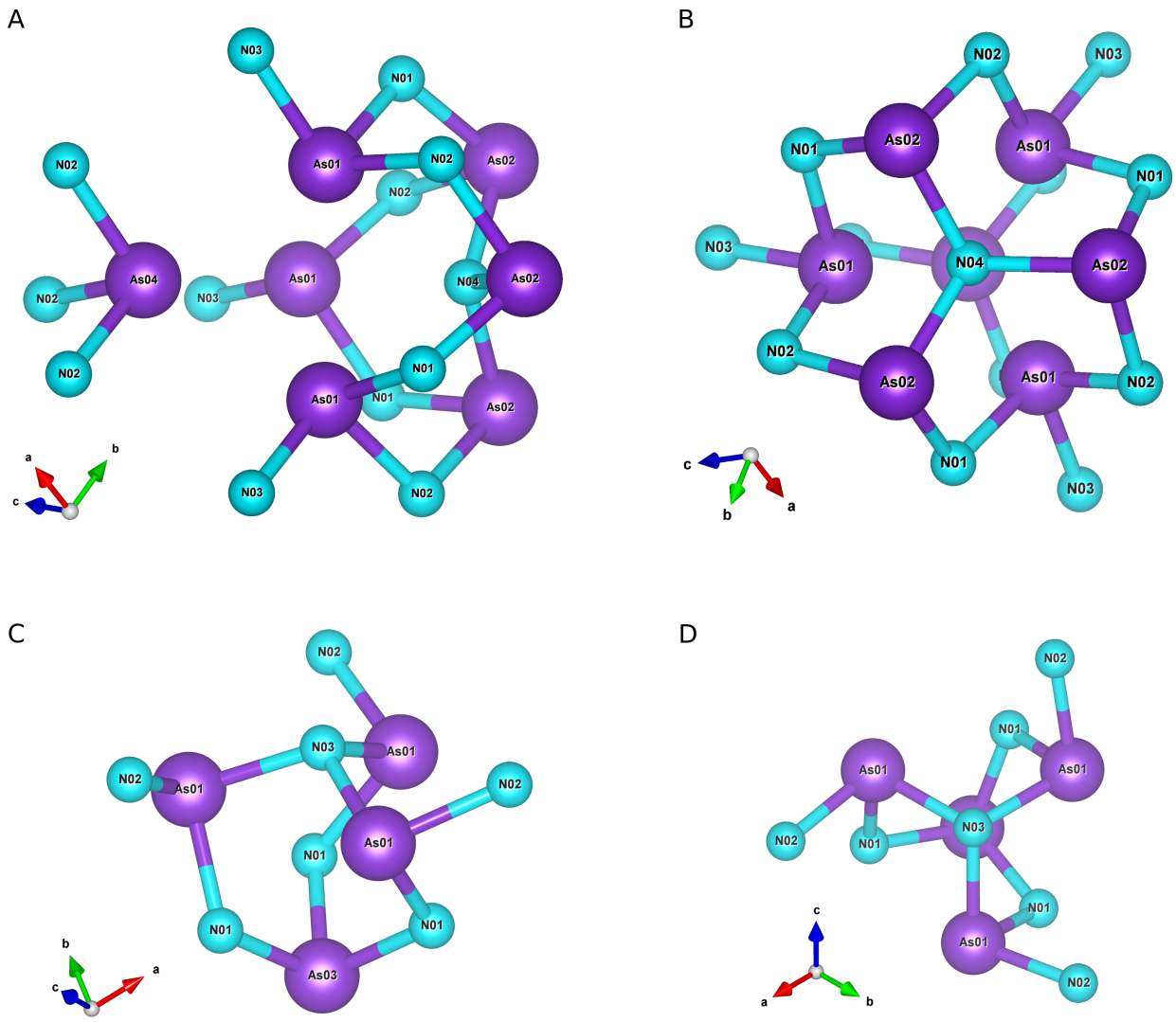

Figure SI-13: Different views of two cage-like structures made of condensed cyclotriarsazene As_3N_3 rings identified along the C_3 axes of the AsN unit cell. Panel A and B: each As_3N_3 ring shares one bond with two other rings and the three rings share a common N atom. Panel C and D: each As_3N_3 ring shares three bonds with two other rings and the three rings share a common As and N atom located on the threefold axis. Data refer to AsN at 35.6 GPa and 293 K

Acknowledgements

Thanks are expressed to EC through the European Research Council (ERC) for funding the project PHOSFUN "Phosphorene functionalization: a new platform for advanced multifunctional materials" (Grant Agreement No. 670173) through an ERC Advanced Grant. This study was supported by the Deep Carbon Observatory (DCO) initiative under the project *Physics and Chemistry of Carbon at Extreme Conditions*, by the project "GreenPhos - alta pressione", by the Italian Ministero dell'Istruzione, dell'Università e della Ricerca (MIUR), and by Fondazione Cassa di Risparmio di Firenze under the project HP-PHOTOCHEM. The authors acknowledge the European Synchrotron Radiation Facility (ESRF) for provision of synchrotron radiation facilities and thank V. Svitlyk, G. Garbarino, M. Mezouar and T. Poreba for assistance in using beamlines ID27 and ID15B (doi 10.15151/ESRF-ES-404440903).

Author contributions

M.C., D.S., M.S.R., Marta Morana., K.D, and R.B. performed the experiments, analyzed all the data and discussed the results. M.P discussed the results. M.S.R. synthesized As. V.S., G.G. and Mohamed Mezouar assisted at ESRF-ID27. G.G. and T.P. assisted at ESRF-ID15B. M.C. conceived the experiment and wrote the article.

Supplementary References

(1) A. P. A P Jeavons, G. A. Saunders, *J. Phys. D Appl. Phys.* **1968**, *1*, 869–873.

(2) Y. Fei, A. Ricolleau, M. Frank, K. Mibe, G. Shen, V. Prakapenka, *Proc. Natl. Acad. Sci.* **2007**, *104*, 9182–9186.

(3) G. Shen, Y. Wang, A. Dewaele, C. Wu, D. E. Fratanduono, J. Eggert, S. Klotz, K. F. Dziubek, P. Loubeyre, O. V. Fat'yanov, P. D. Asimow, T. Mashimo, R. M. M.

Wentzcovitch, other members of the IPPS task group, *High Press. Res.* **2020**, *40*, 299–314.

(4) A. Friedrich, B. Winkler, L. Bayarjargal, W. Morgenroth, E. A. Juarez-Arellano, V. Milman, K. Refson, M. Kunz, K. Chen, *Phys. Rev. Lett.* **2010**, *105*, 085504.

(5) C. Prescher, V. B. Prakapenka, *High Press. Res.* **2015**, *35*, 223–230.

(6) Oxford, UK. Rigaku Oxford Diffraction **2021**.

(7) G. M. Sheldrick, *Acta Cryst. Section A* **2015**, *71*, 3–8.

(8) G. M. Sheldrick, *Acta Crystallogr. C* **2015**, *71*, 3–8.

(9) K. Tolborg, C. Gatti, B. B. Iversen, *IUCrJ* **2020**, *7*, 480–489.

(10) D. Shriver, M. Weller, T. Overton, J. Rourke, F. Armstrong, *Inorganic Chemistry*, W. H. Freeman, 6th ed., **2014**.

(11) K. Momma, F. Izumi, *J. Appl. Cryst.* **2011**, *44*, 1272–1276.